Microfluidic Systems

DOI: 10.1002/ange.201309885

Mesenchymal-Mode Migration Assay and Antimetastatic Drug Screening with High-Throughput Microfluidic Channel Networks**

*Yuanqing Zhang, Weijia Zhang, and Lidong Qin**

Abstract: *Increasing evidence shows that activated mesenchymal migration is a key process of the metastatic cascade. Cancer cells usually gain such migratory capability through an epithelial-to-mesenchymal transition. Herein we present a high-throughput microfluidic device with 3120 microchambers to specifically monitor mesenchymal migration. Through imaging of the whole chip and statistical analysis, we can evaluate the two key factors of velocity and percentage related to cell migratory capacity at different cell densities in culture. We also used the device to screen antimetastatic drugs for their inhibition of mesenchymal migration and prevention of metastatic malignancy. This device will provide an excellent platform for biologists to gain a better understanding of cancer metastasis.*

Metastatic recurrence and chemotherapy resistance are main causes of cancer deaths.[1] The metastatic process involves a cascade of transitions in the cancer-cell phenotype that enable cells to gain invasiveness at the primary site,[2] circulate in the blood or lymphatic system,[3] and interact with the cell microenvironment at the metastatic site.[1,4] The epithelial–mesenchymal transition (EMT) is a central molecular program that enhances cell migration in cancer progression[5] and endows cancer cells with a more motile mesenchymal phenotype that initiates or enhances invasive functions by mesenchymal-mode migration. In many types of cancer, EMT is always associated with the features of cancer stem cells (CSCs) or drug resistance.[6] Therefore, inhibition of mesenchymal-mode cell migration may lead to more effective cancer treatments.[7] Additionally, much evidence has suggested that cell migration is a social behavior and related to cell density in culture.[8] Characterization of mesenchymal-mode migration and quantitation of migratory capability in relation to cell density may provide a powerful tool to more accurately study cell invasiveness.

Traditional techniques for studying cell migration, such as Transwell and wound-healing assays, are endpoint assays and often lack information on migration dynamics and cell-phenotype heterogeneity.[2,11] More desirable features of tools for the measurement of cell invasiveness include real-time monitoring, discrimination of migration modes, tightly controlled gradients, and the requirement for only a small number of sample cells. Quantitation of migratory capability at different cell densities is also very important in providing more accurate characterization of the effects of the microenvironment.[2c,9]

Microfluidic systems, because of their microscale fabrication and high-throughput capabilities, can potentially satisfy such criteria by providing better spatiotemporal resolution and requiring smaller sample volumes, even down to a single cell.[10] Although considerable effort has been directed toward the development of chip-based cell-migration assays over the last decade, quantitative and statistical measurement of cell-migration-related factors remains a challenge. Also, high-throughput screening of mesenchymal-migration inhibitors will require new technological improvements.[11] Herein, we present a high-throughput microfluidic device with 3120 ultraminiaturized chambers, termed the mesenchymal-migration chip (M-Chip), to monitor mesenchymal-mode migration and screen for antimetastatic drugs that specifically inhibit mesenchymal migration. The M-Chip microchamber migration assay enables single-cell resolution and avoids cross-talk between chambers by isolating chambers through multilayered microfluidics-controlled valves. Through statistical analysis, we can study two key factors related to cell migration, that is, the migration velocity of individual cells and the amount of migrating cells as a percentage of the total amount of seeded cells (Figure 1 A). The M-Chip provides a high-throughput platform for biologists to better perform cancer-metastasis-related assays.

The M-Chip is comprised of a two-layer microfluidics network: the flow layer for implementing chemotactic cell migration and the control layer for on-chip valve operation. The device was assembled by carefully aligning two polydimethylsiloxane (PDMS) layers that were then bonded to a $75 \times 50\ mm^2$ glass slide (see Figures S1 and S2 in the Supporting Information). Each individual microchamber is isolated by closing the control valves on top of the flow layer; the center region aligns 10 parallel microchannels to form cell-migration pathways, and microcontainters are placed at the top and bottom of the device for loading cells and chemoattractants (Figure 1 B). The channels measured $10 \times 10 \times 400\ \mu m^3$ ($W \times H \times L$), thus mimicking the capillaries and

[*] Dr. Y. Zhang, Dr. W. Zhang, Prof. L. Qin
Department of Nanomedicine
Houston Methodist Research Institute
6670 Bertner Avenue, Houston, TX 77030 (USA)
and
Department of Cell and Developmental Biology
Weill Medical College of Cornell University
New York, NY 10065 (USA)
E-mail: LQin@tmhs.org

[**] This study was funded by the Cancer Prevention and Research Institute of Texas (CPRIT-R1007), NIH-CA180083, the Emily Herman Research Fund, and the Golfers Against Cancer Foundation. We are grateful for the generous supply of MCF-7 and its derived cell lines by Prof. Mien-Chie Hung.

Supporting information for this article is available on the WWW under http://dx.doi.org/10.1002/anie.201309885.

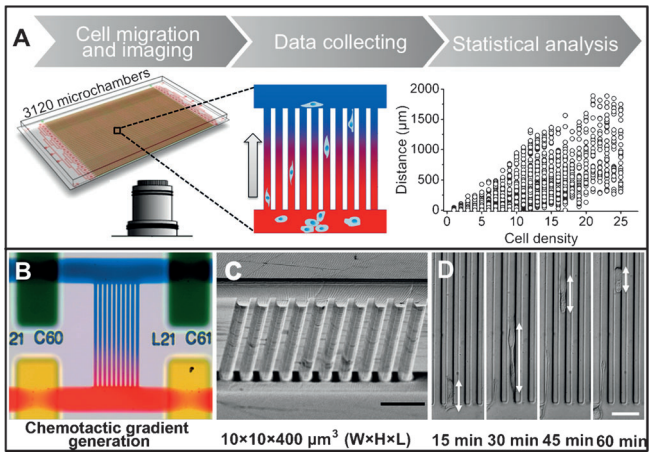

Figure 1. Design and operation of the M-Chip device for mesenchymal-mode cell migration. A) Flowchart of the design, fabrication, and operation of the M-Chip to study cell migration and screen inhibitors. B) Bright-field micrograph of one microchamber showing the chemotactic gradient. C) Scanning electron microscopic image of the microchamber; the microchannel measured $10\times10\times400\ \mu m^3$ (W×H×L). D) Optical micrographs of a SUM-159 tumor cell migrating across a channel taken at 15 min intervals. Scale bars in (C) and (D) are both 50 μm.

pores of tissue or vasculature that allow tumor-cell migration (Figure 1C). The chemoattractant gradient was established in these microchannels and evaluated by the diffusion of bovine serum albumin (BSA) labeled with fluorescein isothiocyanate; BSA is a major component of fetal bovine serum (FBS; see Figure S3). The gradient can be maintained for as long as 4 h under our experimental conditions. When we replaced the medium at 2 h intervals, we always maintained a chemoattractant gradient in the 6 h experiments. This approach also served to reduce the frequency of device operation to minimize potential effects on cell migration. Flow was carefully controlled so as not to disturb the cells (see Figure S4).

We next studied the migration behavior of breast-cancer cells on the M-Chip by using metastatic SUM-159 cell lines as our research model. In the absence of a chemoattractant stimulus, few SUM-159 cells migrated into the channels; the cells appeared to move randomly (see Figure S5). Conversely, after loading 20% FBS as a chemoattractant, we found that the SUM-159 cells demonstrated a clear chemotactic response toward the FBS side. The migration mode in the microchannels was carefully adjusted by regulation of the migration-channel size so that mesenchymal migration was favored, whereas amoeboid migration was avoided.[2] The dimensions of channels intended to allow mesenchymal migration of cells with a diameter of approximately 15 μm or more were adjusted to 10 μm in width and height. In all M-Chip experiments and over thousands of cell-migration chambers, we observed only mesenchymal-mode migration, distinguished by elongated cell morphology with cell polarity (Figure 1D). After cancer cells acquired an elongated morphology, they manifested a strong polarity through the rearrangement of membrane and protein lipids. The cells formed protrusions at their leading edges, toward the higher concentration of the chemoattractant, and retracted their trailing edges, moving forward simultaneously (see Figure S6 and Video S1 in the Supporting Information). After each experiment, all chambers in one chip were photographed under a microscope, and the images were stitched together for the entire device area. The migration distance and percentage of migrating cells in each individual chamber were measured to evaluate migratory capability. Figure 2A,B shows the fluorescence images of SUM-159/GFP cells migrating across channels at 6 h. The trajectory of the migration path was tracked by using the center of the nucleus (or the cell center if the nucleus could not be seen clearly) as the tracking point. The total distance migrated in each chamber was calculated by totaling the distances migrated by all cells in the chamber (Figure 2C). The migration velocity for individual cells was calculated from the distance migrated in 6 h. The average migration velocity was calculated either for a whole chamber or for multiple chambers loaded with the same number of cells, thus suggesting that average velocity is independent of cell density. The average migration velocity of SUM-159 cells in the channels was $15.9\ \mu m\,h^{-1}$ (standard deviation (SD): $6.33\ \mu m\,h^{-1}$). Besides migration velocity, the percentage of migrating cells is an important factor associated with migra-

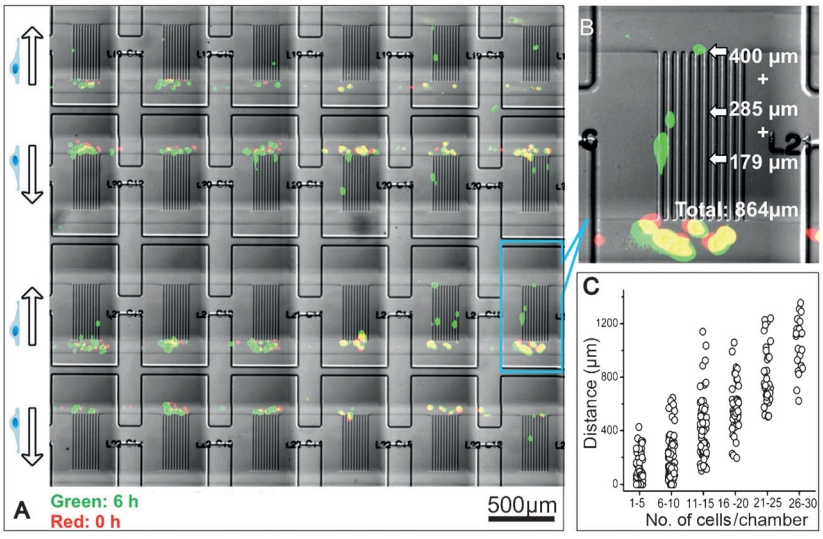

Figure 2. Time-lapse images of SUM-159/GFP cells migrating in microchannels. A,B) Alignment and autofocus scripts were implemented to acquire homogeneous images. The coordinates of the four corners of the array were first determined manually, and then the coordinates for the entire grid were automatically calculated by extrapolation based on the device geometry. C) Statistical analysis of the migration distances of the cells at different cell densities after culture for 6 h on the M-Chip. Red pseudocolor indicates cell position at 0 h, and green indicates position at 6 h. The brightness and contrast of the fluorescence images were adjusted to ensure that the cells could be seen clearly. The channel is a closed system; all cells migrated between the barriers. All experiments were performed at 37°C.

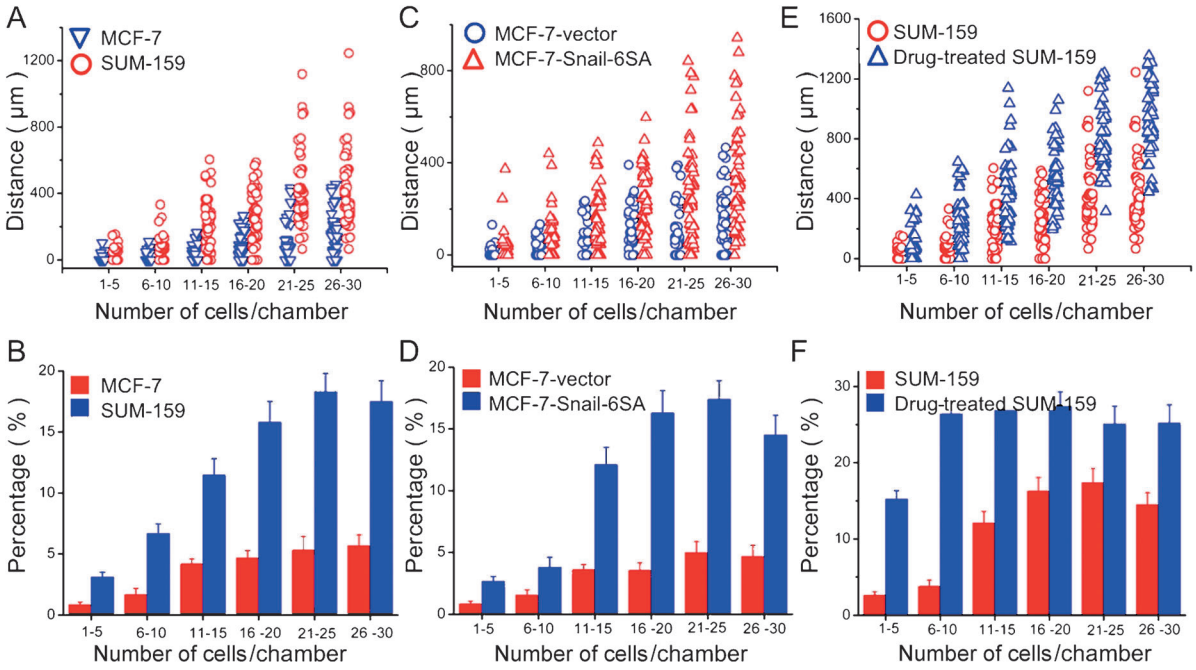

Figure 3. Migratory potential of cells derived from MCF-7 and SUM-159 cell lines. A,C,E) Comparison of the migration distances and B,D,F) percentage of migrating cells for MCF-7 and SUM-159 cells (A and B), MCF-7–vector and MCF-7–Snail-6SA cells (C and D), and parental SUM-159 and drug-resistant SUM-159/Taxol cells (E and F). In (A,C,E), the *y* axis shows the total distance migrated by cells in one chamber. The percentage of cells was calculated for each chamber at different cell densities. All measurements were taken at 6 h. Error bars indicate the standard deviation of replicates ($n = 100$ chambers).

tory capability. The greater the number of cells loaded into an individual chamber, the higher the percentage of cells demonstrating chemotaxis will be (the percentage of migrating cells followed a Gaussian distribution; see Figure S7). We also used MCF-7 cells, a nonmetastatic cancer cell line, to test our device (Figure 3A). The average migratory velocity of MCF-7 cells was 8.4 $\mu m\,h^{-1}$ (SD = 2.67 $\mu m\,h^{-1}$), and the percentage of migrating cells did not increase significantly, even when a greater number of cells was loaded into the chamber (Figure 3B). Notably, the average size of MCF-7 cells (ca. 12 μm in diameter) is smaller than that of SUM-159 cells (ca. 14 μm). Therefore, it is reasonable to expect that MCF-7 cells would pass more easily through the channel. However, the results showed that migratory capacity was not related to cell size.

We also characterized the migratory propensity of cancer cells before and after EMT. The MCF-7 cell line induced by the Snail transcription factor was employed for the assay, and MCF-7 cells transfected with the empty vector were used as a control. The MCF-7 vector-carrying cell is an epithelial cancer cell line that exhibits cobblestone-like morphology (see Figure S8). Cells transfected with Snail-6SA, on the other hand, demonstrated a loss of the epithelial markers E-cadherin and cytokeratin and the gain of the mesenchymal marker vimentin.[12] After image-capture statistical analysis of the cell-migration data, we found that most of the MCF-7–vector cells were not attracted into the channels, and few demonstrated chemotactic behavior (see Figure S9). Conversely, a greater proportion of the MCF-7–Snail-6SA cells entered channels and moved toward the source of the chemoattractant (see Figure S10). On average, MCF-7–Snail-6SA cells migrated farther and faster in channels (Figure 3C; see also Figure S11) than MCF-7–vector cells. We also analyzed the percentage of migrated cells in these two cell lines. Similarly to SUM-159 cells, at a higher cell density, a higher percentage of MCF-7–Snail-6SA cells migrated toward the chemoattractant (Figure 3D). However, MCF-7–vector cells did not show a significant change in the percentage of migrating cells with increasing cell density. These results indicate that after EMT, the enhanced migratory capacity of cancer cells was closely related to cell density in culture, and directional cell migration needed collaboration behavior among cells. Recent evidence indicates that EMT of breast-cancer cells not only causes increased metastasis but also contributes to drug resistance.[6,13] We then used the M-Chip and paclitaxel-treated SUM-159 (SUM-159/Taxol) cells to study the mesenchymal migration behavior of drug-resistant cells. At all cell densities, the migration distance of drug-resistant cells was greater than that of parental cells (Figure 3E). The average velocity of SUM-159/Taxol cells was approximately 27.4 $\mu m\,h^{-1}$ (SD = 13.37 $\mu m\,h^{-1}$). The average migration velocity at different cell densities was also studied; the data indicate that cell density did not have an appreciable effect on migration velocity. In contrast, the proportion of migrating cells changed with cell density. At a lower cell density (1–5 cells/chamber) the percentage of migrating SUM-159/Taxol cells was more than fourfold greater than that of parental SUM-159 cells. In chambers with a higher cell density (> 10 cells/chamber), the percentage of migrating cells was only slightly higher than that of the parental SUM-159 cells (Figure 3F). These results indicate that at lower cell densities, the migratory capacity of drug-

resistant cancer cells depends both on a greater percentage of migrating cells and a higher velocity; at higher cell densities, the migratory capacity depends only on a higher migration velocity. Lower cell density may correspond to the early stage of cancer, and treatment with paclitaxel might increase the proportion of migrating cells, thus enhancing cancer metastasis.[14]

Another important application of the M-Chip is high-throughput screening of mesenchymal-migration inhibitors. In this study, we tested nine small-molecule compounds that inhibit specific chemokines, growth factors, and kinases related to breast-cancer metastasis (see Table S1 in the Supporting Information). To determine the inhibitory potency of these nine compounds, we cultured SUM-159/Taxol cells with these inhibitors for 12 h and then loaded cells into the M-Chip for the mesenchymal-mode migration assay (Figure 4A). The migration distance of cells treated with the nine inhibitors was plotted as a heat map (Figure 4B). Our results indicate that these compounds can be divided into two categories: those that slightly promote cell migration (which was unexpected), and those that inhibit cell migration. Axitinib and drug 444278 belong to the first category. The migratory potential of SUM-159/Taxol cells was slightly enhanced by these two compounds. The other seven compounds reduced the mesenchymal-mode migration distance to different degrees; they reduced either the cell-migration velocity or the percentage of migrating cells. AMD3100, canertinib, drug 227013, and linifanib significantly reduced the velocity of cell migration (see Table S2). The other inhibitors had no effect on velocity. linifanib, PD173074, canertinib, and SB525334 effectively reduced the percentage of migration-competent cells. However, axitinib and drug 444278 increased the proportion of migration-competent cells (Figure 4C). The maximal level of inhibition was seen with linifanib (ABT-869). This compound is a structurally novel, potent inhibitor of the following proteins: RTK, VEGF and PDGF receptor families, and CSF-1R, and reduced both velocity and percentage (see Figure S12). Our screening results are consistent with the findings of other research groups, as the inhibition of TGF-βR and EGFR will reduce the migratory potential of breast-cancer cells.[15] Our device allows more accurate and higher-throughput screening of migration-inhibiting drugs.

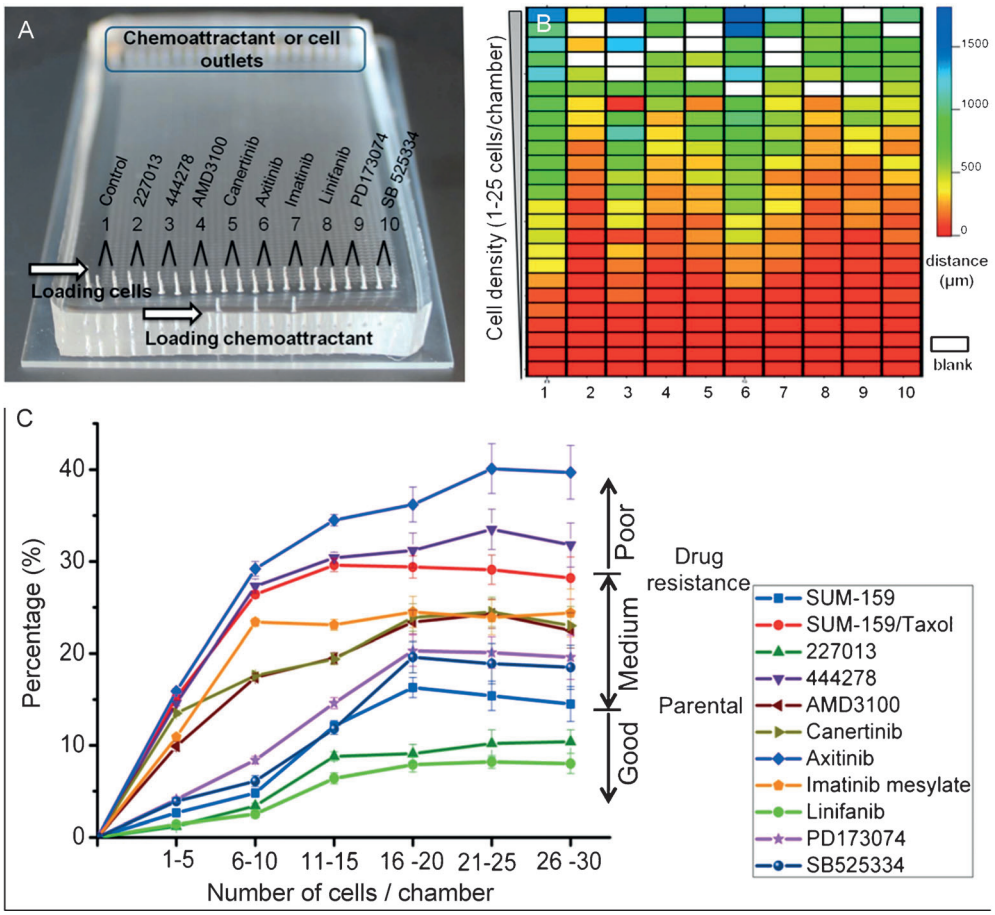

Figure 4. Screening of small-molecule-inhibitor effects on mesenchymal-mode migration. A) Schematic illustration of the loading inlets and outlets of cells and chemoattractants. B) Plotted heat map exhibiting inhibitor-screening results. The vertical axis indicates cell density; the color scale of the heat map indicates the total migration distance of migrated cells in each chamber. C) The percentage of migrated cells inhibited by nine small-molecule compounds. The points indicate the average percentage, which follows a Gaussian distribution. Error bars indicate the standard deviation of replicates ($n = 40$ chambers). The lines connecting points are provided as guidance only. All measurements were taken at 6 h.

In summary, we verified the applicability of the M-Chip for the study of cancer metastasis by performing a mesenchymal-mode migration assay on breast-cancer cell lines at different seeded-cell densities. Average cell-migration velocity and the percentage of migrating cells are two key values generated by the M-Chip assay. By calculating the migration velocity and the percentage of migrating cells in each chamber, we quantified migratory potential over a wide range of cell densities, which may correspond to different stages of malignancy. The small sample size (< 10000 cells; in such cases, we used only one or two of 20 groups of channels by applying cells from the access holes individually) used with the M-Chip enables detection and analysis of the metastatic potential of primary or rare cells. This device provides a high-throughput platform for biologists to better per-

form assays that evaluate cancer-cell behavior related to metastasis.

Received: November 13, 2013
Published online: January 29, 2014

Keywords: cancer · high-throughput screening · mesenchymal-mode migration · metastasis · microfluidics

[1] C. L. Chaffer, R. A. Weinberg, *Science* **2011**, *331*, 1559 – 1564.
[2] a) A. J. Ridley, *Science* **2003**, *302*, 1704 – 1709; b) J. A. Joyce, J. W. Pollard, *Nat. Rev. Cancer* **2008**, *8*, 239 – 252; c) E. T. Roussos, J. S. Condeelis, A. Patsialou, *Nat. Rev. Cancer* **2011**, *11*, 573 – 587.
[3] D. Hanahan, R. A. Weinberg, *Cell* **2000**, *100*, 57 – 70.
[4] I. J. Fidler, *Nat. Rev. Cancer* **2003**, *3*, 453 – 458.
[5] a) K. Polyak, R. A. Weinberg, *Nat. Rev. Cancer* **2009**, *9*, 265 – 273; b) J. P. Thiery, H. Acloque, R. Y. J. Huang, M. A. Nieto, *Cell* **2009**, *139*, 871 – 890.
[6] A. Singh, J. Settleman, *Oncogene* **2010**, *29*, 4741 – 4751.
[7] a) Y. Yui, K. Itoh, K. Yoshioka, N. Naka, M. Watanabe, Y. Hiraumi, H. Matsubara, K.-i. Watanabe, K. Sano, T. Nakahata, S. Adachi, *Clin. Exp. Metastasis* **2010**, *28*, 619 – 630; b) J. Zhong, A. Paul, S. J. Kellie, G. M. O'Neill, *J. Oncol.* **2010**, *2010*, 1 – 17; c) C. R. Mackay, *Nat. Immunol.* **2008**, *9*, 988 – 998.
[8] a) S. Vedel, S. Tay, D. M. Johnston, H. Bruus, S. R. Quake, *Proc. Natl. Acad. Sci. USA* **2012**, *109*, 129 – 134; b) P. Rosen, D. S. Misfeldt, *Proc. Natl. Acad. Sci. USA* **1980**, *77*, 4760 – 4763.
[9] a) P. B. Gupta, C. M. Fillmore, G. Jiang, S. D. Shapira, K. Tao, C. Kuperwasser, E. S. Lander, *Cell* **2011**, *146*, 633 – 644; b) J. Li, F. Lin, *Trends Cell Biol.* **2011**, *21*, 489 – 497.
[10] a) H. N. Joensson, H. Andersson Svahn, *Angew. Chem.* **2012**, *124*, 12342 – 12359; *Angew. Chem. Int. Ed.* **2012**, *51*, 12176 – 12192; b) E. Primiceri, M. S. Chiriaco, F. Dioguardi, A. G. Monteduro, E. D'Amone, R. Rinaldi, G. Giannelli, G. Maruccio, *Lab Chip* **2011**, *11*, 4081 – 4086; c) W. Zhang, K. Kai, D. S. Choi, T. Iwamoto, Y. H. Nguyen, H. Wong, M. D. Landis, N. T. Ueno, J. Chang, L. Qin, *Proc. Natl. Acad. Sci. USA* **2012**, *109*, 18707 – 18712; d) S. Wang, K. Liu, J. Liu, Z. T. Yu, X. Xu, L. Zhao, T. Lee, E. K. Lee, J. Reiss, Y. K. Lee, L. W. Chung, J. Huang, M. Rettig, D. Seligson, K. N. Duraiswamy, C. K. Shen, H. R. Tseng, *Angew. Chem.* **2011**, *123*, 3140 – 3144; *Angew. Chem. Int. Ed.* **2011**, *50*, 3084 – 3088; e) H. Song, J. D. Tice, R. F. Ismagilov, *Angew. Chem.* **2003**, *115*, 792 – 796; *Angew. Chem. Int. Ed.* **2003**, *42*, 768 – 772; f) X. Mu, W. Zheng, J. Sun, W. Zhang, X. Jiang, *Small* **2013**, *9*, 9 – 21.
[11] Y. Huang, B. Agrawal, D. Sun, J. S. Kuo, J. C. Williams, *Biomicrofluidics* **2011**, *5*, 013412 – 013429.
[12] a) H. C. Lien, Y. H. Hsiao, Y. S. Lin, Y. T. Yao, H. F. Juan, W. H. Kuo, M.-C. Hung, K. J. Chang, F. J. Hsieh, *Oncogene* **2007**, *26*, 7859 – 7871; b) B. P. Zhou, J. Deng, W. Xia, J. Xu, Y. M. Li, M. Gunduz, M.-C. Hung, *Nat. Cell Biol.* **2004**, *6*, 931 – 940.
[13] D. Kong, Y. Li, Z. Wang, F. H. Sarkar, *Cancer* **2011**, *3*, 716 – 729.
[14] a) S. Gingis-Velitski, D. Loven, L. Benayoun, M. Munster, R. Bril, T. Voloshin, D. Alishekevitz, F. Bertolini, Y. Shaked, *Cancer Res.* **2011**, *71*, 6986 – 6996; b) I. E. Haines, G. L. Miklos, *N. Engl. J. Med.* **2008**, *358*, 1637; author reply 1637 – 1638.
[15] a) J. T. Price, T. Tiganis, A. Agarwal, D. Djakiew, E. W. Thompson, *Cancer Res.* **1999**, *59*, 5475 – 5478; b) E. Wiercinska, H. P. Naber, E. Pardali, G. Pluijm, H. Dam, P. Dijke, *Breast Cancer Res. Treat.* **2011**, *3*, 657 – 666.